Desalination and Water Treatment
www.deswater.com

doi: 10.5004/dwt.2020.26265

206 (2020) 202–214
December

Mesoporous biochar obtained from coir pith on removing nickel(II) from aqueous simulated solution – batch and column studies

L. Vidhya[a,*], T. Ramya[b,*], S. Vinodha[a]

[a]*Department of Chemical Engineering, Sethu Institute of Technology, Pulloor, Kariapatti, Virudhunagar – 626115, Tamil Nadu, India, Tel. +91 9443938568; emails: vidhuram236@gmail.com (L. Vidhya), vinodha.harris@gmail.com (S. Vinodha)*
[b]*Department of Environmental Sciences, Bharathiar University, Coimbatore – 641046, Tamil Nadu, India, email: rtramya1@gmail.com (T. Ramya)*

Received 3 December 2019; Accepted 10 June 2020

ABSTRACT

Biochar derived from coir pith (C-BC) was initiated for the removal of Ni(II) ions from simulated aqueous solution. C-BC showed higher uptake compared with other adsorbents. The surface morphology and functionality of the C-BC before and after adsorption were characterized using scanning electron microscopy-energy dispersive spectroscopy, Fourier transform infrared spectroscopy, and desorption studies reveals the benefits C-BC. The adsorption capacity was effective of C-BC owing to the results from mesoporous structure and large surface area as well as shift in the FT-IR studies. The adsorption of Ni(II) ions onto C-BC was investigated with the effect of contact time, dosage of adsorbent, initial metal concentration and pH of the of Ni(II) ions solution. The experimental maximum sorption capacity of C-BC for Ni(II) removal was approximately 99.8% at pH 7. Through comparison with other natural seed and plant materials, the optimization of biochar adsorption was well described with kinetics, isotherms, and with column studies. The kinetics was found to follow pseudo-second-order with a good correlation coefficient (R^2 = 0.9704). Langmuir model implies that chemisorption and monolayer adsorption is the rate-limiting steps. They are found to be the satisfactory fit to the equilibrium adsorption data of C-BC (R^2 = 0.9921). In column studies, the breakthrough time increased with increase in bed height and decreased with decrease in flow rate and initial Ni(II) concentration. The column data were modeled by Thomas model, modified dose-response model, and Yoon–Nelson model. The results obtained clearly indicates that C-BC could be used for the removal of Ni(II) from simulated aqueous solution. The maximum adsorption capacity of Ni(II) onto C-BC is 99.8 mg g^{-1}, higher than Ni with an average removal power of 65.75% mg g^{-1} of *Platanus orientalis* bark. C-BC has an excellent energetic and dynamic performance comparing with BC.

Keywords: Adsorption; Coir pith biochar; FT-IR; Fixed bed column kinetic models; Isotherms; Models; Ni(II) ions; SEM-EDAX

1. Introduction

Heavy metals contamination in the environment is an increasing economic, public health, and environmental problem. Industrial wastewaters with elevated concentration of heavy metals cause significant environmental problem because of their mobility in the liquid phase of ecosystems, toxicity to higher life forms, and bio magnifications in the food chain [1]. Nickel (Ni), a heavy metal, commonly present in the discharges from various industries such as

* Corresponding authors.

electroplating, batteries, porcelain enameling, ceramic, mining, metallurgy, and stainless-steel manufacturing plants. Ni contamination in the ecosystem is a disturbing factor for microorganisms, plants, and other biotic communities [2]. Exposure to Ni causes skin allergies, dry cough, lung fibrosis, shortness of breath, rapid respiration, cyanosis, and extreme weakness in human beings. Thus, it is very important to remove the Ni from industrial wastewaters before it is discharged into the ecosystem.

Numerous methods, such as chemical precipitation, coagulation and flocculation, ion exchange, reverse osmosis, and membrane separation, electrochemical reduction, and biological treatment, have been developed to remove Ni from wastewater [3]. However, these technologies are expensive, generate secondary wastes, and remain ineffective when nickel is present in low concentrations. Adsorption, an effective and versatile method for removal of heavy metals is when combined with suitable desorption step solves the problem of sludge disposal. A number of low-cost adsorbents have been examined for the removal of metallic pollutants from wastewaters [4].

Biochar, a carbon-rich fine grained residue, is produced when a biomass is pyrolyzed (<700°C) in the absence of oxygen or under low oxygen pressure. On the whole, the biochar produced at high temperatures displays highly efficient carbon (C) layers and also has strong aromatic nature, but then has fewer H and O functional groups due to dehydration and deoxygenation of the biomass [5]. Recently, biochar has received considerable interest in environmental sciences because of its effectiveness in removing both inorganic and organic pollutants from soil and aqueous solution [6]. Sugar cane biochar removed 86.96 mg g of Pb(II) from aqueous solution [7]. The previous study on biochar states that it is one of the most capable support materials for biosorbent due to its high stability and high metal adsorption capacity owing to its oxygen-rich groups on its surface and porous structure [8]. Biochar is progressively being considered as an alternative agent for isolation of heavy metals in waste water treatment technologies [9].

Biochar prepared from oily seeds of *Pistacia terebinthus* L. removed 3.53 mg g^{-1} of Cr(VI) under optimized conditions [10]. Biochars obtained from peanut, soybean, canola, and rice straws have great adsorption capacities (Q_{max} = 0.48, 0.33, 0.28, and 0.27 mol kg) for Cr(III) [11]. However, the pollutant removal efficiency of the biochar is highly influenced by the physical and chemical properties such as surface functional groups, coordination to p electrons (C=C), carbon content, electrostatic interactions, and insoluble matters, and which is completely depend upon the raw materials used for the biochar preparation.

The most of the earlier studies on heavy metals adsorption onto biochar were restricted to batch experiment studies. However, such basic information's could not be applicable for large or industrial scale applications where the contact time is not sufficient to attain equilibrium. Thus, it is necessary to evaluate the metal removal efficiency of the biochar in continuous flow system or fixed-bed column study before its application in wastewater treatment at large scale. Several investigators have identified that the fixed-bed column studies are most efficient arrangement for cyclic adsorption–desorption as it provides the best use of concentration gradient known to be the driving force of adsorption. Furthermore, fixed-bed column studies are economical, highly sensitive, and simple to operate and easily adapted to large or industrial-scale treatment. Hence, the objectives of the present study were to (i) investigate the potential of the coir pith biochar (C-BC) for the removal of Ni(II) from aqueous solution in batch and fixed-bed column studies, (ii) evaluate the experimental variables on Ni(II) adsorption onto C-BC in batch experiments, (iii) assess the experimental parameters such as column bed height, flow rate, and initial metal concentration for process optimization in column studies, (iv) and analyze the experimental data's with common dynamic models to understand the mechanism and efficiency of Ni(II) adsorption onto C-BC.

2. Materials and methods

2.1. Samples and materials

Coir pith waste was collected from Thondamuthur village of Coimbatore, Tamil Nadu, India. The waste materials were washed with deionized water, oven dried (60°C for 24 h), and used for the production of biochar using a small scale biochar producing plant (Safire Scientific Company, Tamil Nadu Agriculture University, Coimbatore, Tamil Nadu, India) [12]. The produced biochar were sieved (<0.25 mm) and used for the batch experiments and column studies. A stock solution of Ni(II) (1,000 mg L^{-1}) was prepared by dissolving 4.478 g $NiSO_4 \cdot 6H_2O$ in deionized water. Working concentrations (50 and 250 mg L^{-1}) solutions were prepared by diluting the stock solution. All other chemicals used in the experiments were of analytical grade.

2.1.1. Point of zero charge of the adsorbent

Consequently, the point of zero charge (pHpzc) for C-BC was determined. About 0.05 g of C-BC was taken in 50 mL Erlenmeyer flasks containing 0.01 mol L^{-1} $NaNO_3$ solutions. Alternatively, the pH values of the solutions were adjusted between 2.0 and 8.0 using the solutions of HNO_3 and NaOH. Further, the mixtures were kept in a shaker to equilibrate at 25°C for 24 h, and the final pH was noticed after 24 h [6].

2.2. Batch experiments

Batch experiments were performed using 0.05 g of C-BC agitated with 25 mL of Ni(II) solution individually at 26°C ± 2°C in a rotary shaker at 100 rpm [10]. Samples were collected at the predetermined time intervals, and the Ni(II) solution was separated from the adsorbent by centrifugation at 6,000 rpm for 5 min [13]. The supernatant was analyzed for the residual Ni(II) concentration using UV-vis spectrophotometer (Hach make: DR/2400 model) at 470 nm. The Ni(II) removal (%) was calculated using the following equation:

$$\text{Removal capacity}\ (\%) = \left[\frac{(C_0 - C_e)}{C_0}\right] \times 100 \quad (1)$$

where C_0 and C_e are the initial and equilibrium Ni(II) concentrations (mg L^{-1}), respectively. All the experiments were

carried out in duplicate to avoid any discrepancy in experimental results and metal solution controls were kept throughout the experiment. Experimental variables considered were (i) the effect of pH 2–8 on the adsorption capacities, (ii) dosage of C-BC (0.05–0.25 g), and (iii) initial Ni(II) concentration (50–250 mg L^{-1}).

2.3. Modeling of adsorption isotherms

The adsorption isotherm studies were performed at equilibrium conditions, in order to determine the relationship between the amount of metal ions adsorbed on the adsorbent surface and the concentration of remaining metal ions in the aqueous phase. Langmuir [Eq. (2)], Freundlich [Eq. (3)], and Temkin [Eq. (4)] isotherms were plotted by using standard straight line equations and corresponding two parameters of Ni(II) was calculated from their respective graphs. The Langmuir isotherm is based on the monolayer sorption of metal ions on the surface of the sorbent and is represented by the following equation [14].

$$\frac{C_e}{q_m} = \left(\frac{1}{q_m b}\right) + \left(\frac{1}{q_m}\right) C_e \tag{2}$$

where C_e is the concentration of metal ions in mg L^{-1} at equilibrium, q_m is the maximum capacity of the metal monolayer to be adsorbed in mg g^{-1}, and b is the constant that refers to the bonding energy of adsorption in L mg^{-1}. Freundlich equation can be expressed as:

$$\log q_e = \log K_F + \frac{1}{n} \log C_e \tag{3}$$

where C_e is the equilibrium concentration of metal ion (mg L^{-1}), q_e is the amount of metal ion adsorbed per unit weight of adsorbed at equilibrium (mg g^{-1}), n is the Freundlich constant and K_F is the adsorption capacity (mg g^{-1}). K_F and n can be determined from a linear plot of $\log q_e$ against $\log C_e$ [15].

The linearized form of Temkin equation is expressed as:

$$q_e = B_T \ln K_T + B_T \ln C_e \tag{4}$$

where $B_T = RT/b$, C_e is the equilibrium concentration of a metal in solution (mg L^{-1}), q_e the amount of Cr(VI) sorbed onto the C-BC (mg g^{-1}), K_T (L g^{-1}) the equilibrium potential corresponding to maximum binding energy, B_T (J mol^{-1}) the Temkin constant relates to the heat of sorption, R the gas constant (8.314 J mol K^{-1}), and T the absolute temperature (K).

2.4. Adsorption kinetics

The first-order rate constant for adsorption of Ni(II) has been studied with the help of Lagergran's equation.

$$\log\left(q_e - q_t\right) = \log\left(q_e\right) - \left(\frac{k_1}{2.303}\right) t \tag{5}$$

where q_e is the amount of metal adsorbed at equilibrium (mg g^{-1}), q_t is the amount of metal adsorbed at time t (mg g^{-1}), k_1 is the rate constant of adsorption (min^{-1}).

Pseudo-second-order rate equation is expressed as:

$$\frac{t}{q_t} = \frac{1}{k_2 q_e^2} + \left(\frac{1}{q_e}\right) t \tag{6}$$

where k_2 is the second-order rate constant for adsorption (g mg^{-1} min^{-1}), q_e is the amount of metal adsorption at equilibrium (mg g^{-1}), and q_t is the amount of metal adsorption in time t (min^{-1}). A plot of t/q_t vs. t yields a straight line with a slope of $1/q_e$. The value of k_2 is determined from the intercept of the plot [16].

2.5. Characterization of C-BC

Fourier transform-infrared spectroscopic analysis was used to identify functional groups responsible for Ni(II) adsorption onto C-BC. Briefly, infrared spectra of Ni(II) loaded and unloaded C-BC were recorded on a Schimadzu, FTIR-8400 spectrometer, Japan, equipped with software-IR Solution. The absorbance data were obtained in the range of 400–4,000 cm^{-1} [17]. The surface morphology of the C-BC before and after Ni(II) adsorption were examined using scanning electron microscopy (SEM), the corresponding SEM micrographs being obtained using at an accelerating voltage of 15 kV (Hitachi SE 900, Ibaraki, Japan) at 5,000× magnification. The surface elemental composition of C-BC before and after Ni(II) adsorption was recorded on a Quanta FEI 250 (Czechoslovakia) equipment.

2.6. Column study

The experimental arrangement for fixed-bed column study consists of the columns of burette connecting to a peristaltic pump and the overhead tank containing aqueous Ni(II) solution of varied concentrations. The known amount of C-BC was packed up to a desired bed height in the column. Columns are mounted vertically and glass wool is used at the bottom of the column to act as supporting material of the adsorbent bed and also serves the purpose of filtration of the adsorbent particles. Control valves of the peristaltic pump after the overhead tank helps to regulate the flow and a graduated burette to measure the influent liquid flow rate are incorporated in the feed line of the column. At the top of the column, the influent nickel solution (50, 75, and 100 ppm) was pumped through the packed column (10, 15, and 20 cm), at flow rates of 1, 2, and 3 mL min^{-1}, using a peristaltic pump. Samples were collected from the exit of the column at standard time intervals and analyzed for residual Ni(II) concentration. All the experiments carried out at the room temperature 26°C ± 2°C. All experiments were carried out in duplicates and mean values are used for the data analysis.

2.7. Mathematical modeling of column data

Breakthrough curves obtained at different bed heights, flow rates, and initial Ni(II) concentration were analyzed

using common dynamic models such as Thomas model, modified dose response model, and Yoon–Nelson model. Thomas model is expressed as:

$$\frac{C_t}{C_0} = \frac{1}{1+\exp\left[\frac{k_T}{F}\left(q_0 m - C_0 V\right)\right]} \tag{7}$$

where k_T is the Thomas rate constant mL min^{-1} mg^{-1}, C_t is the equilibrium concentration (mg L^{-1}) at time t (min), q_0 is the maximum column adsorption capacity (mg g^{-1}), V is the cumulative throughput volume (dm^3), F is the volumetric flow rate (L min^{-1}) and C_0 is the initial nickel concentration (mg L^{-1}). The Thomas model is the resultant of the concept based on the following theory: (a) Langmuir adsorption/desorption, (b) no axial dispersion, (c) the rate driving force follows second-order reversible reaction kinetics [18].

The modified dose-response model is expressed as:

$$\frac{C_t}{C_0} = 1 - \frac{1}{1+\left(F_t/b\right)1+\left(F_t/b\right)^{\text{amdr}}} \tag{8}$$

where amdr and b are the modified dose-response model constants [19], C_t is the equilibrium concentration (mg L^{-1}) at time t (min), q_0 is the maximum column adsorption capacity (mg g^{-1}), and C_0 is the initial nickel concentration (mg L^{-1}). From the value of b, the value of q_0 can be estimated using the following equation.

$$q_0 = \frac{bC_0}{m} \tag{9}$$

where m is the mass of adsorbent (g).

The Yoon–Nelson model is based on the statement that the rate of decrease in the probability of adsorption for each adsorbate molecule is proportional to the probability of adsorbate adsorption and the probability of adsorbate breakthrough on the adsorbent. The linear equation model for a single component system is expressed as:

$$\ln\left[\frac{C_t}{C_0 - C_t}\right] = k_{\text{YN}} - \tau k_{\text{YN}} \tag{10}$$

where k_{YN} is the rate constant (per min), τ is the time required for 50% adsorbate breakthrough (min).

A plot in the form of linear is expressed as $\ln[C_t/(C_0 - C_t)]$ against sampling time (t). It was used to establish the values of k_{YN} and τ from the intercept and slope of the plot. In the linear plot a general equation of the form $y = a - bt$ is obtained from which the values of k_{YN} and τ are obtained by equating a = and $b = k_{\text{YN}}$ [18].

3. Results and discussion

This study represents an attempt to assess the potential of C-BC for removing Ni(II) from aqueous solution. The high carbon content (61%), good particle size ratio (1.00), low moisture content (0.27%), and ash content (16%) indicate the good adsorptive capacity of the C-BC. The physicochemical properties of the C-BC are depicted in Table 1.

3.1. Effect of nickel concentration

Effect of initial concentration was studied by varying the Ni(II) concentration from 50 to 250 mg L^{-1} with 0.05 g of adsorbent (at a contact time interval of 10 min) and the results are depicted in Fig. 1. In all the experiments, a rapid removal was observed during the first 30 min and gradually decreased with laps of time until it reaches the equilibrium. The maximum removal (99.8%) was observed for 100 mg L^{-1} and minimum removal (71.6%) was observed for 250 mg L^{-1}. Thus, the concentration 100 mg L^{-1} was taken as optimum concentration for further experiments. The enhanced removal at low concentration could be due to the faster movement of Ni(II) ions into the reactive sites of C-BC. However, the decreased removal in higher concentrations (200 and 250 mg L^{-1}) was due to the fact that adsorbents had a fixed number of active sites, which become saturated above a certain concentration [20,21]. The good adsorption can be attributed to two main factors like high probability of collision between metal ions and the sorbent surface and high diffusion rate of metal ions onto sorbent surface [22,23].

3.2. Effect of adsorbent dosage

The effect of adsorbent dosage (0.01–0.05/25 mL) on Ni(II) removal was evaluated and the results are depicted in Fig. 2. The concentration of Ni(II) and pH were kept at 100 ppm and 7, respectively. The maximum removal 99.6% of nickel was observed at 0.05 g and minimum removal 92.9% was observed for 0.01 g. Thus, further experiments were carried out with 0.05 g C-BC, as it removed 99.6% of Ni(II) from aqueous solution. The percentage removal of Ni(II) ions increases due to the increase in the adsorbent dosage. This is mainly due to an increase in the biosorption binding sites. At a high adsorbent dose, all active sites of the C-BC are fully exposed and occupied by the Ni(II) ions saturating the surface and yielding higher adsorption value [24]. The results are consistent with previous studies reporting the increased metals adsorption according to increase in the adsorbent dose [19].

3.3. Effect of pH

The pH of the solution is an important variable which controls the adsorption of the metal ions at the solid-water interface by altering surface properties of the adsorbent and the ionic form of the metal solution [3,25]. Thus, the 0.05 g of C-BC was mixed with 25 mL of Ni(II) solutions at different pH values (2–8), and the results are depicted in Fig. 3. The pH of the solution was altered after the addition of C-BC. From the graph, it was observed that the Ni(II) adsorption of Ni(II) takes place at all pH ranges from 2 to 8 and the maximum adsorption efficiency (99.6%) was observed at pH 7. When the pH value is increased the maximum adsorption at pH 7 could be due to the protonation of both amine and carboxyl groups in the C-BC, eventually the negative charge present in the surface increases, thus favoring the adsorption of Ni(II) ions. This occurs due to the reduction of electrostatic repulsion between the surface and metal cations eventually leading to strong electrostatic

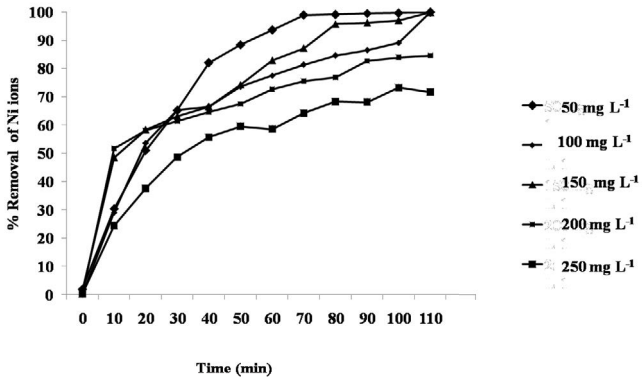

Fig. 1. Effect of concentration on the removal of Ni(II) onto C-BC. The Ni(II) removal was decreased with increased initial concentration.

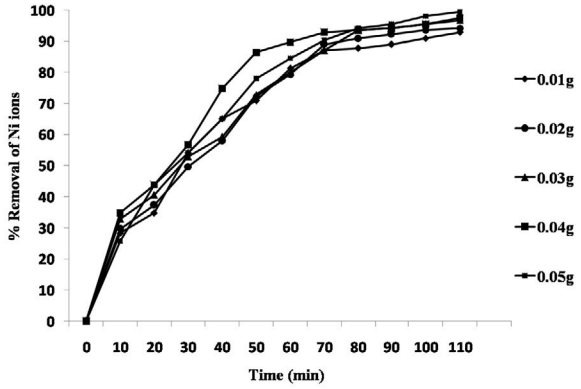

Fig. 2. Effect of dosage on the removal of Ni(II) onto C-BC. A minor increase in adsorption capacity was observed with increased adsorbent dose.

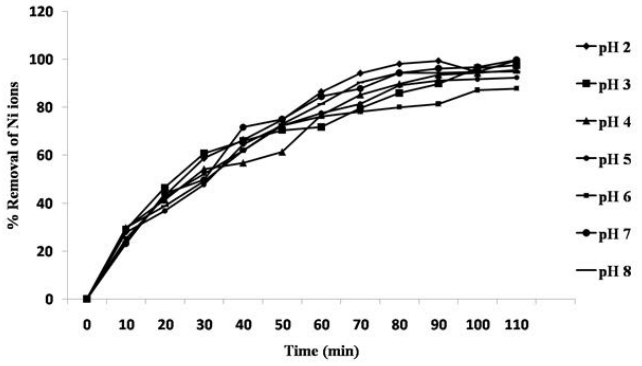

Fig. 3. Effect of pH on the removal of Ni(II) onto C-BC. The maximum adsorption (99.8%) was observed at pH 7.

attraction between the Ni(II) ions and C-BC [26]. When the pH is lower (pH < pHpzc), the adsorbent surface will have positive form and will have the lesser adsorption. Due to the increase in alkalinity of the solution, the carboxylic acid functional groups changes into carboxylate anions and the adsorption increases progressively till pH > pHpzc. After that, carboxylic acid functional groups completely get converted into carboxylate anions, with nearly no change in adsorption [27]. However, deprotonation of carboxylic group in acidic pH (3–6) may faintly decrease the Ni(II) adsorption onto C-BC. Thus, further experiments were carried out at neutral pH 7. The results are in accordance with previous study who reported Cd adsorption onto peanut husk biochar at neutral pH [28].

When the pH is low, the adsorbent surface will acquire positive charge and the adsorption is less. Once the alkalinity of solution is increased, the carboxylic acid functional groups turn into carboxylate anions and the adsorption increases gradually until pH > pHpzc. At the end, carboxylic acid functional groups completely turn into carboxylate anions, with virtually no change in adsorption. Hence, increase in the pH of the solution depicts the different effects on the adsorption process. This can be demonstrated by the point that Ni(II) species hydrolyzes and it is precipitated into $Ni(OH)_2$ at pH 7.0 [27].

3.4. Adsorption isotherms

The Langmuir, Freundlich, and Temkin isotherm models were widely used to describe the interaction between metal ions in solution and adsorbents [15]. The Langmuir isotherm is valid for monolayer adsorption onto a surface containing a finite number of identical binding sites. The maximum absorption occurs when the adsorbent surface is covered by a single molecular layer of soluble material. The absorption energy is fixed and identical at all the points. The molecules or ions of adsorbed material cannot move in the adsorbent surface [29]. In Langmuir isotherms, R_L values indicate whether the isotherm is favorable or not and it is calculated using the following formula:

$$R_L = \frac{1}{\left(1 + b\,C_0\right)} \tag{11}$$

The adsorption data were analyzed according to the isotherm Eq. (2) and the important parameters are reported in Table 1. The Langmuir plot is shown in the Fig. 4. Langmuir constant (q_m) and affinity constant (R_L) were used to compare the results, and it represents the adsorption capacity of the adsorbent. The results reveal that the C-BC had higher Q_{max} and the R_L values as compared to the other biochars [30]. The adsorbent with high Q_{max} and R_L values were usually advantageous for the waste-water treatment process [31].

Freundlich isotherm illustrates the factor $1/n$ which implies the favorability of adsorption. The high K_F values depicts the high affinity of C-BC toward Ni(II) ions, while low K_F values indicates low adsorption rate of metal ion [32]. Table 2 reveals that though the values of $1/n$ were good for Ni(II) ions, the K_F values of Freundlich isotherm do not fit the adsorption data. The Temkin adsorption isotherm model was chosen to evaluate the adsorption potentials of the adsorbent for the adsorbate. By comparing the linear correlation coefficients (R^2) of the three isotherms studied, it was found that the Langmuir isotherm described the equilibrium data well with high R^2 value 0.9921 (Table 2).

Table 1
Physico-chemical properties of coir-pith biochar

S. no	Characteristics	Result
1	pH	7.7
2	EC (ds m^{-1})	2.87
3	Water holding capacity (%)	193.41
4	Moisture content (%)	0.27
5	Volatile content%	18
6	Fixed carbon content%	61
7	Ash content%	16
8	Zeta potential (mV)	–26.3
9	Particle size (SP area ratio)	1.00
10	Surface area	m^2 g^{-1}
	300°C	1.00
	400°C	6.22
	600°C	87.5
11	Porosity	cm^3 g^{-1}
	300°C	0.011
	400°C	0.020
	600°C	0.085

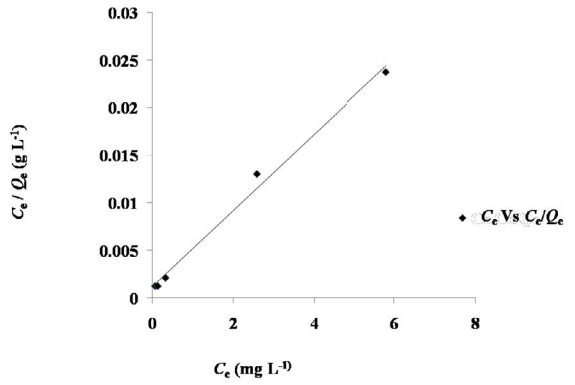

Fig. 4. Langmuir isotherm for concentration of Ni(II) adsorption by C-BC at pH = 7, dosage = 0.05 g.

The results indicate that Ni(II) adsorption proceeds by monolayer sorption formation [33]. Also, it implied that C-BC had a high affinity for Ni(II) ions in solution. Table 3 depicts the comparison of maximum adsorption capacities of different adsorbents with the present study.

3.5. Kinetic model

The kinetic study of the adsorption processes often used to describe the efficiency of adsorption and the potential rate controlling step in the adsorption system. The kinetics study was completed in 110 min with initial Ni(II) concentrations (50–250 mg L^{-1}) using 0.05 g of C-BC at 25°C [26]. Pseudo-first-order and pseudo-second-order were used to model the kinetic data. The validity of the kinetic model is usually checked by the correlation coefficient (R^2), calculated from the linear plots. The R^2 values are more close to 1.0, indicating a better fit to the model [49]. In this study, R^2 values pseudo-second-order model (0.9704) was close to 1.0 indicating the better fit of the model [50] (Table 4). The pseudo-second-order plot is shown in Fig. 5. It was found that, the equilibrium sorption capacities determined using pseudo-second-order model was in agreement with the experimentally determined equilibrium sorption capacities (Table 4). In general, the adsorption reaction was known to proceed the following: (1) transfer of adsorbate from bulk solution to adsorbent surface, (2) migration of adsorbate into pores, and (3) interaction of adsorbate with available sites on the interior surface of pores.

Table 2
Isotherm model constants for Ni(II) ion adsorption onto coir-pith biochar

Isotherm models	Parameters	Values
Langmuir model	q_m (mg g^{-1})	249.733
	K_L (L mg^{-1})	3.372604
	R_L	
	50 mg L^{-1}	0.005895
	100 mg L^{-1}	0.002956
	150 mg L^{-1}	0.001973
	200 mg L^{-1}	0.00148
	250 mg L^{-1}	0.001185
	R^2	0.992119
Freundlich model	K_F (mg g^{-1}) (L $mg^{-1})^{1/n}$	156.7607
	n	3.323
	R^2	0.8565
Temkin model	K_T	84.742
	B_T	39.0362
	R^2	0.9775

3.6. Characterization of C-BC

Representative scanning electron micrograph of the C-BC before and after Ni(II) adsorption is shown in Figs. 6a and b. The C-BC has irregular shape with granular surface, which play a vital role in Ni(II) adsorption process [28]. However, the nature of C-BC was altered after Ni(II) adsorption and suggested that Ni(II) effectively interacted with C-BC. Ni(II) adsorption onto C-BC was further confirmed by energy-dispersive spectroscopy (EDS) analysis. Before adsorption, the EDS pattern for C-BC did not show the characteristic signal of Ni, whereas, after sorption, a clear signal of Ni was observed at 0.4 keV (Figs. 7a and b) [51].

The two chief physical properties that has impact over the metal sorption capacity of biochar are surface area and porosity. After the pyrolysis of C-BC, the micro pores were formed in biochar this is due to the loss of water in dehydration process. Biochar pore has various sizes and incorporates nano- (<0.9 nm), micro- (<2 nm), and macro-pores (>50 nm). The most important factor for metal sorption is pore size. The biochar with small pore size will not capture bulky sorbate, irrespective of their charges or polarity. Both these two physical properties will differ significantly with temperature. The studies in the present research reveals that higher temperature usually leads to

Table 3
Comparison of maximum adsorption capacity (q_m) (mg g^{-1}) of different adsorbents for Ni(II) ions

Adsorbent	Metal ions	Q_{max} (mg g^{-1})	Reference
Activated carbon from *Hevea brasiliensis*	Ni(II)	16.892	Rozaini et al. [34]
Activated carbon from lotus stalk	Ni(II)	31.45	Huang et al. [35]
Cyanobacterium *Oscillatoria laetevirens*	Ni(II)	84.745	Das [36]
Jackfruit (*Artocarpus heterophyllus*) leaf powder	Ni(II)	11.5	Boruah et al. [37]
Palm fibers	Ni(II)	4.42	Boudaoud et al. [38]
Platanus orientalis	Ni(II)	285.714	Sheida Akar et al. [39]
Novel chelating sponge	Ni(II)	65.39	Cheng et al. [40]
Magnetic graphenes	Ni(II)	158.5	Guo et al. [41]
Multi-carboxyl-functionalized silica gel	Ni(II)	31.92	Li et al. [42]
Magnetite nanorods	Ni(II)	95.42	Karami [43]
Chelating resin	Ni(II)	62.79	Chen et al. [44]
Bagasse fly ash	Ni(II)	6.48	Srivastava et al. [45]
Activated carbon from scrap tire	Ni(II)	19.53	Gupta et al. [46]
Coal dust	Ni(II)	20.408	Kapur and Mondal [47]
Peat	Ni(II)	61.27	Przemysław Bartczak et al. [48]
C-BC	Ni(II)	249.733	Present research work

List of comparison of the adsorption capacity of other materials

Table 4
Adsorption kinetic model constants for Ni(II) adsorption onto coir-pith biochar

Kinetic models	Parameters	Initial concentration (ppm)				
		50	100	150	200	250
Pseudo-first-order	$q_{e,exp}$ (mg g^{-1})	49.9355	99.871	149.6775	197.42	244.195
	$q_{e,calc}$ (mg g^{-1})	44.65517	120.2368	187.3268	189.3485	509.0483
	k_1 (min^{-1})	–0.0463	–0.03269	–0.04084	–0.02498	–0.03676
	R^2	0.780826	0.819031	0.938445	0.610672	0.754937
Pseudo-second-order	$q_{e,exp}$ (mg g^{-1})	49.9355	99.871	149.6775	197.42	244.195
	$q_{e,cal}$ (mg g^{-1})	58.05755	109.5936	166.2146	181.8138	231.9527
	k_2 (g mg^{-1} min^{-1})	0.000883	0.000452	0.000372	0.000321	0.000175
	R^2	0.970423	0.960158	0.969428	0.949036	0.905098
	h	0.051253	0.049589	0.0061783	0.058431	0.040549

$q_{e,exp}$ values are obtained from the experiment. It is the value of adsorption capacity at equilibrium condition.

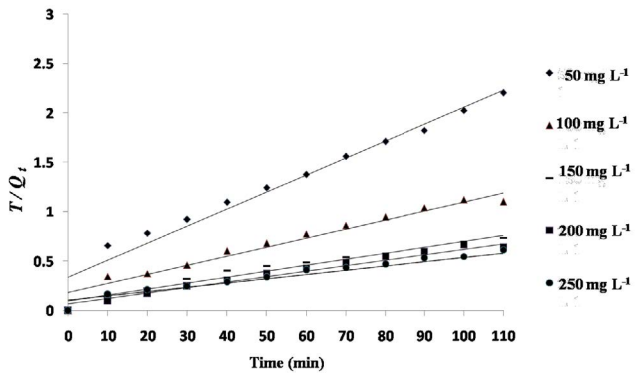

Fig. 5. Ho's pseudo-second-order kinetic plots for adsorption of Ni(II) by C-BC.

bigger pore size, thus larger surface area (Table 1). The temperature is increased from 300°C to 600°C, porosity of C-BC increased from 0.011 to 0.085 cm^3 g^{-1}, while surface area gets increased from 1.0 to 87.5 m^2 g^{-1}. But it must be noticed that, in some cases, biochar produced at high temperature shows lower surface area and porosity. In a previous study [52], it was observed that reduced surface area for biochar produced from wheat straw at 700°C compared to that at 600°C (363 vs. 438 m^2 g^{-1}). Generally, at high temperature, the porous structure of biochar might be damaged or obstructed by tar, which leads to decreased surface area. Usually, the biochar which is rich in lignin develops macroporous-structured biochar, while the biochar rich in cellulose yields a predominantly microporous-structured biochar [53].

Numerous functional groups such as sulfhydryl, alkyl, hydroxyl, aryl, carboxyl, keto, phosphonate, sulfonate, and

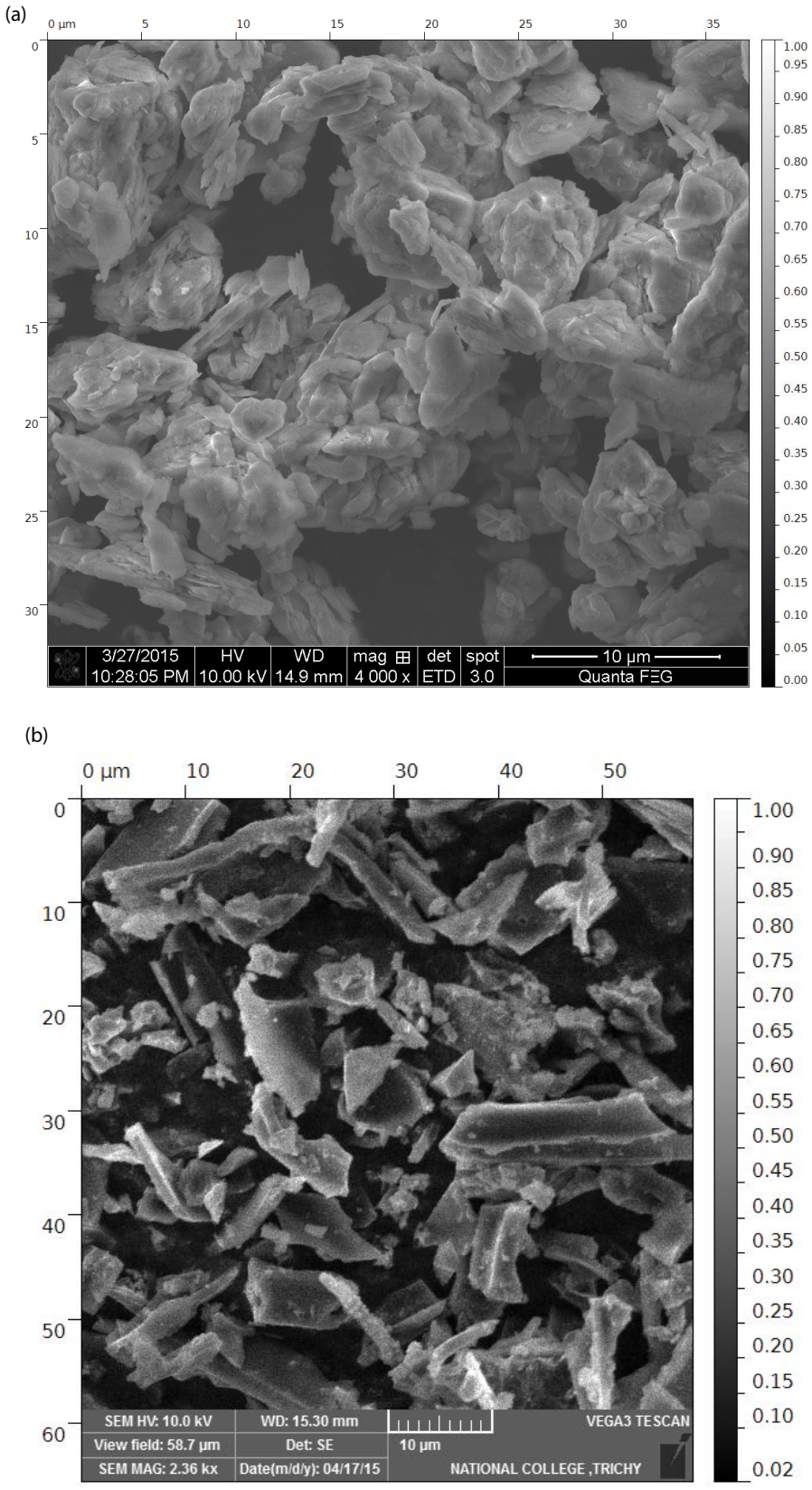

Fig. 6. Scanning electron micrographs of coir-pith biochar before and after Ni(II) adsorption. The C-BC has irregular plates with numerous mesopores over the surface. (a) before adsorption and (b) after Ni(II) adsorption.

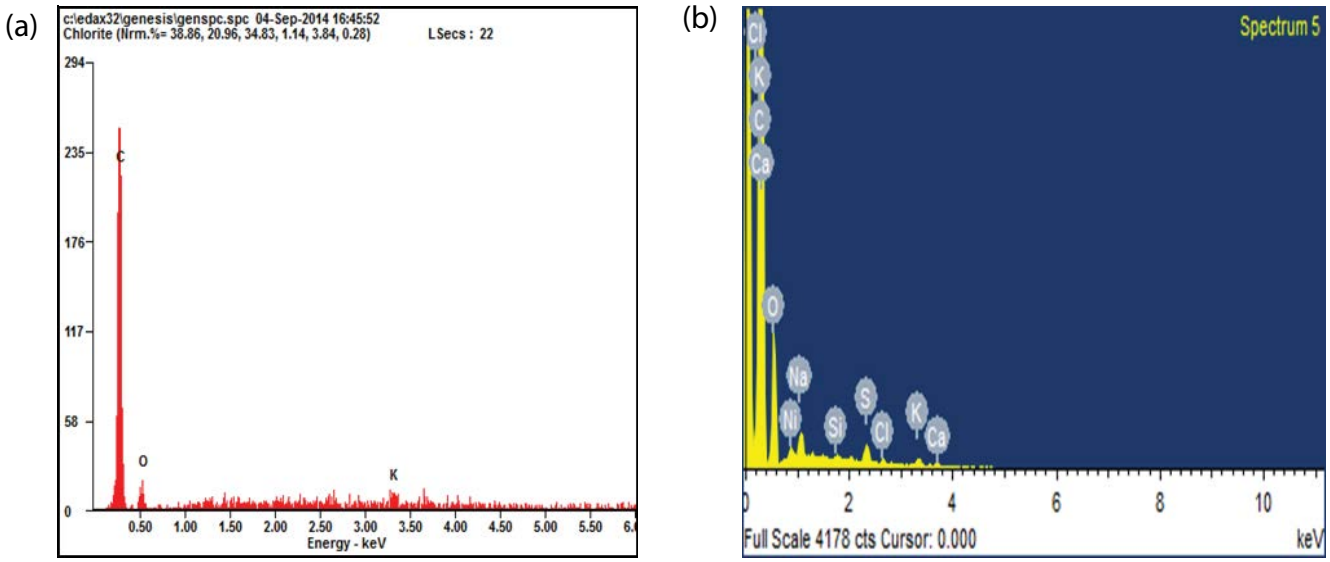

Fig. 7. Energy dispersive spectrum of C-BC (a) before and (b) after Ni(II) adsorption.

amide groups are thought to contribute to the adsorbtion of metal ions in biochar. Thus, to understand the functional groups involved in the adsorption of Ni(II) ions in C-BC, Fourier-transform infrared (FTIR) analysis was carried out, and the results are shown in Fig. 8. The spectra were plotted using the same scale on the transmittance axis for C-BC before and after adsorption. The FTIR spectra of the C-BC display number of adsorption peaks, indicating the complex nature [54]. The basic changes observed in the spectrum before and after Ni(II) binding on C-BC indicated the influence of different functional groups on Ni(II) adsorption process. The wave number 2,854 cm^{-1} was assigned to the C–H stretch aldehyde groups. The shift at 1,689 to 1,627 cm^{-1} indicates the presence of carboxylic acid salts [55]. The change in the peak from 1,442 to 1,389 cm^{-1} depicts the presence of C–C aromatics. The peak at 879 shows the bonding of C–H bending thereby indicating presence of alkyl group in adsorption process.

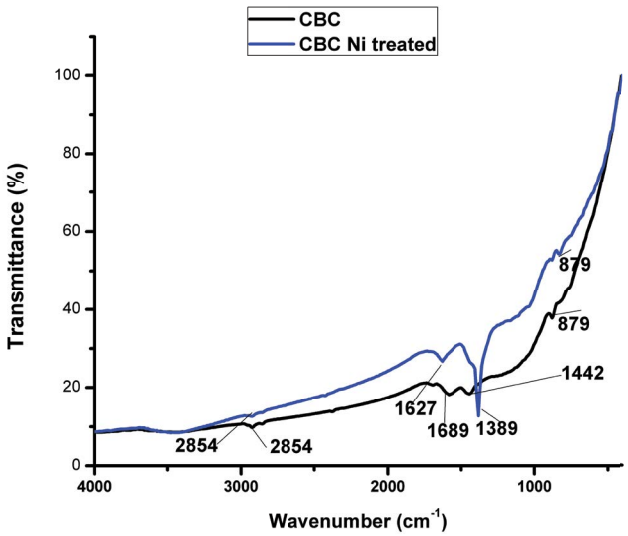

Fig. 8. FT-IR spectra of C-BC before and after Ni(II) adsorption. A minor shift in the carboxyl group was observed in Ni(II) treated C-BC.

3.7. Effect of bed height

Breakthrough curves obtained for Ni(II) adsorption onto C-BC at various bed heights are shown in Fig. 9. Bed heights of 10, 15, and 20 cm were maintained with weighed amount of 2.5, 3.5, and 5.5 g of biochar, respectively. The uptake of Ni(II) increased with an increase in bed height from 10 to 20 cm. The metal ion has the breakthrough and exhaustion time increased with an increase in bed height as more binding sites were available for sorption. It also resulted in a broadened mass transfer zone (Table 3). The *S*-curve has the slope decreased as its bed height increased from 10 to 20 cm, signifying the breakthrough curve steeper as the bed height decreased. On the other hand, with an increase in bed height, the abode time of Ni(II) solution inside the column was increased, thus making the nickel ions to distribute deeper into the C-BC.

3.8. Effect of flow rate

The effect of flow rate for the adsorption of Ni(II) onto the C-BC at flow rates of 1, 2, and 3 mL min^{-1}, at an inlet Ni(II) concentration of 50 mg L^{-1} and bed height of 20 cm is shown in Fig. 10. The figure notifies that rapid uptake of nickel ion in the initial stages and rate decreased thereafter and finally reached the saturation [56]. Increase in flow rate makes the breakthrough curves steeper and it rapidly reached the breakthrough. This is because of the residence time of the adsorbate in the column, which is time-consuming for adsorption equilibrium to be reached at high flow rate. The contact time between the adsorbate and the adsorbent is minimized which leads to the early breakthrough.

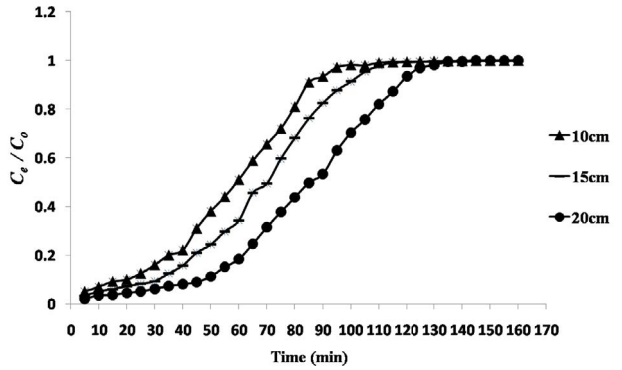

Fig. 9. Breakthrough curves expressed as C_e/C_0 vs. time at different bed depth (initial nickel concentration 50 mg L^{-1} initial pH 7, flow rate 1 mL min^{-1}, and temperature 20°C ± 1°C) on C-BC.

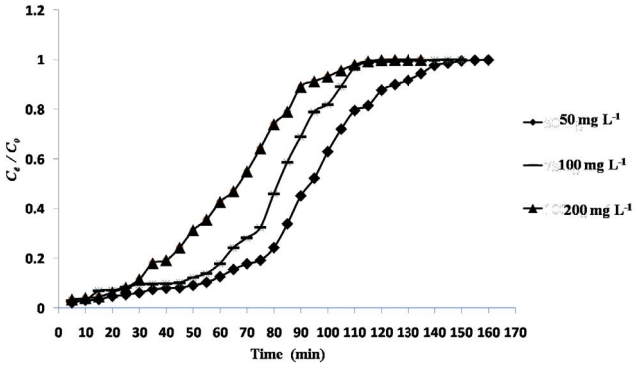

Fig. 11. Breakthrough curves expressed as C_e/C_0 vs. time at different inlet concentrations (flow rate 1 mL min^{-1}, initial pH 7, bed height 20 cm, and temperature 20°C ± 1°C) on C-BC.

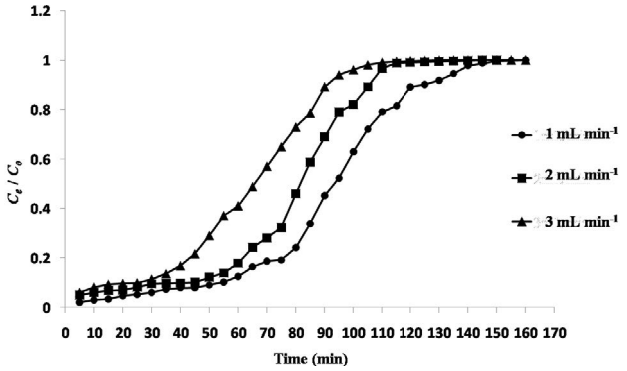

Fig. 10. Breakthrough curves expressed as C_e/C_0 vs. time at different flow rate (initial nickel concentration 50 mg L^{-1}, initial pH 7, bed height 20 cm, and temperature 20°C ± 1°C) on C-BC.

3.9. Effect of concentration

The breakthrough curve obtained for the effect of inlet initial Ni(II) concentration at bed height 20 cm and solution flow rate of 1 mL min^{-1} is shown in Fig. 11. At 100 min, for inlet initial concentrations of 50, 75, and 100 mg L^{-1}, the value of C_e/C_0 reached 0.63, 0.82, and 0.94 respectively. Due to the increasing driving force and the decrease of adsorption zone length, the slope of breakthrough is steeper with the larger inlet concentration. The results corroborate with previous fixed-bed column studies reporting high adsorption of Pb(II). A steeper breakthrough slope due to increase in driving force and decrease in adsorption zone length with larger inlet concentration was reported earlier [57].

3.10. Dynamic adsorption models

The Thomas model illustrates adsorption kinetics of fixed bed column. Table 5 illustrates the Thomas rate constant k_{Th} and the maximum solid phase concentration Q_0 and the correlation coefficient R^2 (ranged between 0.994 and 0.996). Owing to the increase in mass transport resistance, the values of k_{Th} decreased with increasing inlet concentration of Ni(II) while the values of Q_0 were increasing. This may be due to the difference in the inlet concentrations between Ni(II) on the C-BC adsorbent surface and in the solution. The adsorption capacity Q_0 decreases with increase in bed height and flow rate. As a result, more adsorption sites were available for Ni(II) ions. A similar study was already reported [58]. The external and internal diffusions were not limiting step on the fitness of this model for adsorption process. Increased flow rate and initial concentration maximizes the adsorption capacity, Q_0 but minimizes with increase in bed height. This study is in agreement with k_{Th} values [59] and with for regression coefficient [60].

The experimental data also fitted well with modified dose-response model as evident from the breakthrough curves shown (Table 5). It was observed in this study that the modified dose-response constants a_{MDR} and b_{MDR} decreased with an increase in initial nickel concentration and flow rate. The R^2 values ranged between 0.978 and 0.986. The modified dose-response model reduces the error, especially with lower and higher breakthrough curve times [61].

The breakthrough time and rate constants of this Yoon–Nelson model are presented in Table 5. Increased rate constant and decreased breakthrough time was noticed with substantial increase in Ni(II) inlet concentration. Moreover, the rate constant considerably increases with increase in flow rate and decreases with increase in bed height. At higher bed height, the Ni(II) molecules had more time to establish through the column, which had reduced adsorption rate. This result is consistent with the previous study of adsorption of Pb(II) Ions using mixture of clay plus bamboo biochar. Decreased rate constant was recorded with increased bed height and breakthrough time [62]. In this study, The R^2 values ranged between 0.98 and 0.99. On comparing the values of R^2 of the three models studied, Thomas and Yoon–Nelson models can better be used for the adsorption of Ni(II) on to C-BC in a fixed bed column. The results corroborate an earlier finding that the R^2 values of modified-dose response model was lower than the other two models when a column study was conducted with reference to adsorption of copper on to rice husk [63].

Table 5
Modified-dose response, Thomas, and Yoon–Nelson model parameters at different flow rates, bed heights, and adsorbate solution inlet concentrations

Kinetic model	Flow rate			Bed height			Initial concentration		
	1 mL min^{-1}	2 mL min^{-1}	3 mL min^{-1}	10 cm	15 cm	20 cm	50 ppm	75 ppm	100 ppm
Modified-dose response model									
a_{MDR}	6.6275	6.831	4.6227	4.1283	4.7626	5.2449	6.675	6.8319	4.239
b_{MDR}	0.0916	0.158	0.1867	0.0559	0.066	0.0825	0.0916	0.0794	0.06154
R^2	0.9869	0.978	0.9785	0.9796	0.9845	0.9852	0.9869	0.9798	0.9781
Thomas model									
K_{TH}	0.0013	0.0016	0.0013	0.0007	0.0013	0.0012	0.0013	0.001	0.0006
Q_0	0.842	1.457	1.7401	1.0509	0.9666	0.7662	0.842	1.0932	1.1616
R^2	0.994	0.988	0.9938	0.9956	0.9968	0.9958	0.994	0.9892	0.9952
Yoon–Nelson model									
τ	92.616	80.15	63.804	57.798	67.661	84.2804	92.6161	80.1671	63.8594
K_{YN}	0.0671	0.077	0.0663	0.0658	0.0658	0.0599	0.06711	0.0781	0.0643
R^2	0.994	0.988	0.9938	0.9956	0.9968	0.9958	0.994	0.9892	0.9952

3.11. Desorption studies

The desorption studies were conducted to consider the suitability of adsorbent (C-BC). In this respect, 0.05 g of C-BC is added to 15 mL of Ni(II) solution concentration of 100 mg L^{-1}, and the mixture was shaken on a shaker. The adsorbents in the mixture were separated, and the Ni(II) ions adsorbed onto C-BC was added into 6 mL of ethanol. To end with, the concentration of Ni(II) ions in the solution was measured by inductively coupled plasma optical emission spectrometry. The desorption efficiency of C-BC was 98.56% for Ni(II) ions (Fig. 10). In addition to this, the desorption of Ni(II) ions onto C-BC, was carried up to five turns without any decrease in the stability of the adsorbents. The most important factor is the reusability of adsorbents which is used to assess their probable applications. Consequently, it is essential to repeat the use of an adsorbent with further appropriate conditions. Moreover, the results revealed the competences of the recycled adsorbent for the isolation of heavy metal ions and it is found that they are closely the same as those with the fresh adsorbent even after recycling five times [27]. Finally, all the results indicated that the adsorbent depicts good performance for flaunting Ni(II) ions.

4. Conclusion

C-BC efficiently removed (>99%) of Ni(II) from aqueous solution. Batch studies revealed a maximum removal of Ni(II) at pH 7. FTIR studies clearly demonstrated the ionic interaction between Ni(II) and the functional groups of C-BC. Scanning micrographs confirmed the mesoporous nature of the C-BC that helps absorb the Ni(II) ions more efficiently. All the column study experiment results well fitted the three mathematical models, viz. modified-dose response model, Thomas model, and Yoon–Nelson model. It gave a linearly fitted equation. In short, the flow rate and bed height influences the adsorption of Ni(II) ions on to C-BC. This suggests that C-BC can efficiently be used to remove heavy metal, especially Ni(II), from aqueous solution. Also, the use of C-BC in remediation in the environment may reduce the problem of coir-pith waste by the coir industries.

Acknowledgments

The first author is grateful to the Departments of Environmental Science of the PSG College of Arts and Science, Coimbatore and of the Tamil Nadu Agricultural University, Coimbatore, and the Department of Chemistry, National College, Tiruchirappalli for providing facilities and extending cordial gestures during the course of her doctoral programme through this study.

References

[1] R.B. Nessima, A.R. Bassiouny, H.R. Zakia, M.N. Moawada, K.M. Kandeel, Biosorption of lead and cadmium using marine algae, Chem. Ecol., 27 (2011) 579–594.
[2] R. Sudha, K. Srinivasan, Nickel(II) removal using modified *Citrus limettioides* peel, Int. J. Environ. Sci. Technol., 12 (2015) 3993–4004.
[3] O. Olasunkanmi, A.E. Okoronkwo, A.F. Aiyesanmi, E.F. Olasehinde, T.S. Adepoju, Biosorption of cadmium(II) and chromium(VI) from aqueous solution by chemically modified *Tithonia diversyfolia* biomass, J. Am. Sci., 10 (2014) 10–18.
[4] M.A. Hossain, H. Ngo, W.S. Guo, T.V. Nguyen, Removal of copper from water by adsorption onto banana peel as bioadsorbent, Int. J. Geomate, 2 (2012) 227–234.
[5] A.U. Rajapaksha, S.S. Chen, D.C.W. Tsang, M. Zhang, M. Vithanage, S. Mandal, B. Gao, N.S. Bolan, Y.S. Ok, Engineered/designer biochar for contaminant removal/immobilization from soil and water: potential and plication of biochar modification, Chemosphere, 148 (2016) 276–291.
[6] A.H. Omidi, M. Cheraghi, B. Lorestani, S. Sobhanardakani, A. Jafari, Biochar obtained from cinnamon and cannabis as effective adsorbents for removal of lead ions from water, Environ. Sci. Pollut. Res., 26 (2019) 27905–27914.

[7] A.A. Abdelhafez, J. Li, Removal of Pb(II) from aqueous solution by using biochars derived from sugar cane bagasse and orange peel, J. Taiwan Inst. Chem. Eng., 61 (2016) 367–375.
[8] J. Shang, M. Zong, Y. Yu, X. Kong, Q. Du, Q. Liao, Removal of chromium(VI) from water using nanoscale zerovalent iron particles supported on herb-residue biochar, J. Environ. Manage., 197 (2017) 331–337.
[9] M.I. Inyang, B. Gao, Y. Yao, Y. Xue, A. Zimmerman, A. Mosa, P. Pullammanappallil, Y.S. Ok, X. Cao, A review of biochar as a low-cost adsorbent for aqueous heavy metal removal, Crit. Rev. Environ. Sci. Technol., 46 (2016) 406–433.
[10] H. Deveci, Y. Kar, Adsorption of hexavalent chromium from aqueous solutions by biochars obtained during biomass pyrolysis, J. Ind. Eng. Chem., 19 (2013) 190–196.
[11] J. Pan, J. Jiang, R. Xu, Adsorption of Cr(III) from acidic solutions by crop straw derived biochars, J. Environ. Sci., 25 (2013) 1957–1965.
[12] S. Shenbagavalli, S. Mahimairaja, Production and characterization of biochar from different biological wastes, Int. J. Plant Agric. Sci., 2 (2012) 2231–4490.
[13] C. Vargas, F.B. Pedro, J. Agerda, E. Castillo, Bio adsorption using compost: an alternative for removal of chromium(VI) from aqueous solutions, Bioresources, 7 (2012) 2711–2727.
[14] M. Anbia, M. Haqshenas, Adsorption studies of Pb(II) and Cu(II) ions on mesoporous carbon nitride functionalized with melamine-based dendrimer amine, Int. J. Environ. Sci. Technol., 12 (2015) 2649–2664.
[15] W.P. Putra, A. Kamari, S. Najiah M. Yusoff, C.F. Ishak, A. Mohamed, N. Hashim, I.M. Isa, Biosorption of Cu(II), Pb(II) and Zn(II) ions from aqueous solutions using selected waste materials: adsorption and characterization studies, J. Encapsulation Adsorpt. Sci., 4 (2014) 25–35.
[16] A. Gupta, R. Yadav, P. Devi, Removal of hexavalent chromium using activated coconut shell and activated coconut coir as low cost adsorbent, J. Inst. Integr. Omics Appl. Biotechnol., 2 (2011) 8–12.
[17] R. Gill, Q. Nadeem, R. Nadeem, R. Nazir, S. Nawaz, Biosorption capacity of vegetable waste biomass for adsorption of lead and chromium, J. Biodivers. Environ. Sci., 5 (2014) 306–317.
[18] J. Datta, U. Mishra, S. Chakraborty, Removal of chromium by column study using tea factory waste as adsorbent, Int. J. Civil Environ. Eng., 35 (2013) 1127–1136.
[19] A.B. Albadarin, C. Mangwandi, A.H. Al-Muhtaseb, G.M. Walker, S.J. Allen, M.N.M. Ahmad, Modelling and fixed bed column adsorption of Cr(VI) onto orthophosphoric acid-activated lignin, Chin. J. Chem. Eng., 20 (2012) 469–477.
[20] A.A. Werkneh, N.G. Habtu, H.D. Beyene, Removal of hexavalent chromium from tannery wastewater using activated carbon primed from sugarcane bagasse: adsorption/desorption studies, Am. J. Appl. Chem., 2 (2014) 128–135.
[21] G. Singh, T. Senapati, D. Prakash, N. Baba, Study on cadmium(II) biosorption by water hyacinth biomass, Int. J. Civil Eng., 3 (2016) 152–154.
[22] L. Wang, Z. Chen, J. Yang, F. Ma, Pb biosorption by compound bioflocculant: performance and mechanism, Desal. Water Treat., 53 (2015) 421–429.
[23] K.G. Vinod, A. Rastogi, A. Nayak, Adsorption studies on the removal of hexavalent chromium from aqueous solution using a low cost fertilizer industry waste material, J. Colloid Interface Sci., 341 (2010) 135–141.
[24] S. Akar, B. Lorestani, S. Sobhanardakani, M. Cheraghi, O. Moradi, Surveying the efficiency of *Platanus orientalis* bark as biosorbent for Ni and Cr(VI) removal from plating wastewater as a real sample, Environ. Monit. Assess., 191 (2019) 373, doi: 10.1007/s10661-019-7479-z.
[25] M. El Batouti, A.-M.M. Ahmed, Adsorption kinetics of nickel(II) onto activated carbon prepared from natural adsorbent rice husk, Int. J. Technol. Enhancements Emerging Eng. Res., 2 (2014) 145–148.
[26] S. Sobhanardakani, R. Zandipak, 2,4-Dinitrophenylhydrazine functionalized sodium dodecyl sulfate-coated magnetite nanoparticles for effective removal of Cd(II) and Ni(II) ions from water samples, Environ. Monit. Assess., 187 (2015) 4635, doi: 10.1007/s10661-015-4635-y.
[27] S. Sobhanardakani, R. Zandipak, Synthesis and application of $TiO_2/SiO_2/Fe_3O_4$ nanoparticles as novel adsorbent for removal of Cd(II), Hg(II) and Ni(II) ions from water samples, Clean Technol. Environ. Policy, 19 (2017), doi: 10.1007/s10098–017–1374–5.
[28] Q. Cheng, Q. Huang, S. Khan, Y. Liu, Z. Liao, G. Li, Y.S. Ok, Adsorption of Cd by peanut husks and peanut husk biochar from aqueous solutions, Ecol. Eng., 87 (2016) 240–245.
[29] S. Dowlatshahi, A.R.H. Torbati, M. Loloei, Adsorption of copper, lead and cadmium from aqueous solutions by activated carbon prepared from saffron leaves, Environ. Health Eng. Manage. J., 1 (2014) 37–44.
[30] S. Chowdhury, M. Yasin, M.T. Uddin, M.A. Islam, Batch and continuous (fixed bed column) adsorption of methylene blue by rubber leaf powder, Int. J. Integr. Sci. Technol., 2 (2016) 24–28.
[31] J. Mao, S.W. Won, K. Vijayaraghavan, Y.S. Yun, Immobilized citric acid-treated bacterial biosorbents for the removal of cationic pollutants, Chem. Eng. J., 162 (2010) 662–668.
[32] S. Arivoli, V. Marimuthu, T. Ravichandran, M. Hema, Kinetics, equilibrium and mechanistic studies of nickel adsorption on a low cost activated calcite powder, Indian J. Sci. Res. Technol., 1 (2012) 41–49.
[33] C. Sukumar, V. Janaki, S.K. Kannan, V. Shanthi, Biosorption of chromium(VI) using *Bacillus subtilis* SS-1 isolated from soil samples of electroplating industry, Clean Technol. Environ. Policy, 16 (2014) 405–413.
[34] C.A. Rozaini, K. Jain, C.W. Oo, K.W. Tan, L.S. Tan, A. Azraa, K.S. Tong, Optimization of nickel and copper ions removal by modified mangrove barks, Int. J. Chem. Eng. Appl., 1 (2010) 84–89.
[35] L.H. Huang, Y.Y. Sun, T. Yang, L. Li, Adsorption behavior of Ni(II) on lotus stalks derived active carbon by phosphoric acid activation, Desalination, 268 (2011) 12–19.
[36] S. Das, Biosorption of chromium and nickel by dried biomass of cyanobacterium *Oscillatoria laete-virens*, Int. J. Environ. Sci., 3 (2012) 341–352, doi: 10.6088/ijes.2012030131032.
[37] P. Boruah, A. Sarma, K.G. Bhattacharyya, Removal of Ni(II) ions from aqueous solution by using low cost biosorbent prepared from jackfruit (*Artocarpus heterophyllus*) leaf powder, Indian J. Chem. Technol., 22 (2015) 322–327.
[38] A. Boudaoud, M. Djedid, M. Benalia, C. Ad, N. Bouzar, H. Elmsellem, Removal of nickel(II) and cadmium(II) ions from wastewater by palm fibers, Chem. Chem. Eng. Biotechnol. Food Ind., 18 (2017) 391–406.
[39] S. Akar, B. Lorestani, S. Sobhanardakani, M. Cheraghi, O. Moradi, Surveying the efficiency of *Platanus orientalis* bark as biosorbent for Ni and Cr(VI) removal from plating wastewater as a real sample, Environ. Monit. Assess., 191 (2019) 373, https://doi.org/10.1007/s10661-019-7479-z.
[40] C. Cheng, J.N. Wang, X. Yang, A.M. Li, C. Philippe, Adsorption of Ni(II) and Cd(II) from water by novel chelating sponge and the effect of alkali-earth metal ions on the adsorption, J. Hazard. Mater., 264 (2014) 332–341.
[41] X.Y. Guo, B. Du, Q. Wei, J. Yang, L.H. Hu, L.G. Yan, W.Y. Xu, Synthesis of amino functionalized magnetic graphenes composite material and its application to remove Cr(VI), Pb(II), Hg(II), Cd(II) and Ni(II) from contaminated water, J. Hazard. Mater., 278 (2014) 211–220.
[42] M. Li, M.-y. Li, C.-g. Feng, Q.-x. Zeng, Preparation and characterization of multi-carboxyl-functionalized silica gel for removal of Cu(II), Cd(II), Ni(II) and Zn(II) from aqueous solution, Appl. Surf. Sci., 314 (2014) 1063–1069.
[43] H. Karami, Heavy metal removal from water by magnetite nanorods, Chem. Eng. J., 219 (2013) 209–216.
[44] C.-Y. Chen, C.-L. Chiang, C.-R. Chen, Removal of heavy metal ions by a chelating resin containing glycine as chelating groups, Sep. Purif. Technol., 54 (2007) 396–403.
[45] V.C. Srivastava, I.D. Mall, I.M. Mishra, Equilibrium modelling of single and binary adsorption of cadmium and nickel onto bagasse fly ash, Chem. Eng. J., 117 (2006) 79–91.

[46] V.K. Gupta, A.N. Suhas, S. Agarwal, M. Chaudhary, I. Tyagi, Removal of Ni(II) ions from water using scrap tire, J. Mol. Liq., 190 (2014) 215–222.
[47] M. Kapur, M.K. Mondal, Competitive sorption of Cu(II) and Ni(II) ions from aqueous solutions: kinetics, thermodynamics and desorption studies, J. Taiwan Inst. Chem. Eng., 45 (2014) 1803–1813.
[48] P. Bartczak, M. Norman, Ł. Klapiszewski, N. Karwańska, M. Kawalec, M. Baczyńska, M. Wysokowski, J. Zdarta, F. Ciesielczyk, T. Jesionowski, Removal of nickel(II) and lead(II) ions from aqueous solution using peat as a low-cost adsorbent: a kinetic and equilibrium study, Arabian J. Chem., 11 (2018) 1209–1222.
[49] C. Lib, H. Wang, Y. Zhang, Pb(II) removal from aqueous solution by cold KOH activated biochar of camphor leaves: isotherms, kinetics and thermodynamics, Desal. Water Treat., 161 (2019) 327–336.
[50] C.A. Igwegbe, P.C. Onyechi, O.D. Onukwuli, I.C. Nwokedi, Adsorptive treatment of textile wastewater using activated carbon produced from *Mucuna pruriens* seed shells, World J. Eng. Technol., 4 (2016) 21–37.
[51] I. Ullah, R. Nadeem, M. Iqbal, Q. Manzoor, Biosorption of chromium onto native and immobilized sugarcane bagasse waste biomass, Ecol. Eng., 60 (2013) 99–107.
[52] Y. Chun, G. Sheng, C.T. Chiou, B. Xing, Compositions and sorptive properties of crop residue-derived chars, Environ. Sci. Technol., 38 (2004) 4649–4655.
[53] H. Li, X. Dong, E.B. da Silva, L.M. de Oliveira, Y. Chen, L.Q. Ma, Mechanisms of metal sorption by biochars: biochar characteristics and modifications, Chemosphere, 178 (2017) 466–478.
[54] A.A. Attia, S.A. Khedr, S.A. Elkholy, Adsorption of chromium ion (VI) by acid activated carbon, Braz. J. Chem. Eng., 27(2010) 183–193.
[55] G. Socrates, Infrared and Raman Characteristic Group Frequencies Tables and Charts, John Wiley and Sons, Ltd., New York, NY, 2004.
[56] J.T. Nwabanne, P.K. Igbokwe, Adsorption performance of packed bed column for the removal of lead(II) using oil Palm fibre, Int. J. Appl. Sci. Technol., 2 (2012) 106–115.
[57] V.C. Taty-Costodes, H. Fauduet, C. Porte, Y.S. Ho, Removal of lead(II) ions from synthetic and real effluents using immobilized *Pinus sylvestris* sawdust: adsorption on a fixed column, J. Hazard. Mater., 123 (2005) 135–144.
[58] A.H. Alamin, L. Kaewsichan, Adsorption of Pb(II) Ions from aqueous solution in fixed bed column by mixture of clay plus bamboo biochar, Walailak J. Sci. Technol., 13 (2016) 949–963.
[59] P. Sivakumar, P.N. Palanisamy, Adsorption studies of basic Red-29 by a non-conventional activated carbon prepared from *Euphorbia antiquorum* L., Int. J. Chem. Technol. Res., 84 (2009) 502–510.
[60] A. Baek, K. Song, S. Kang. Y. Rhee, C. Lee, B. Lee, S. Hudson, T. Hwang, Adsorption kinetics of boron by anion exchange resin in packed column bed. J. Ind. Eng. Chem., 13 (2007) 452–456.
[61] S.V. Gokhale, K.K. Jyoti, S.S. Lele, Modeling of chromium(VI) biosorption by immobilized *Spirulina platensis* in packed column, J. Hazard. Mater., 170 (2009) 735–743.
[62] P.D. Rocha, A.S. Franca, L.S. Oliveira, Batch and column studies of phenol adsorption by an activated carbon based on acid treatment of corn cobs, Int. J. Eng. Technol., 7 (2015) 459–464.
[63] N.K.E.M. Yahayaa, I. Abustana, M.F.P.M. Latiffa, O.S. Bello, M.A. Ahmad, Fixed-bed column study for Cu(II) removal from aqueous solutions using rice husk based activated carbon, Int. J. Eng. Technol., 11 (2011) 186–190.